This article has been accepted for publication in a future issue of this journal, but has not been fully edited. Content may change prior to final publication. Citation information: DOI 10.1109/TIP.2015.2468183, IEEE Transactions on Image Processing

Gradient Domain Guided Image Filtering

Fei Kou, Weihai Chen, *Member, IEEE,* Changyun Wen, *Fellow, IEEE,* Zhengguo Li, *Senior member, IEEE*

***Abstract*—Guided image filter (GIF) is a well-known local filter for its edge-preserving property and low computational complexity. Unfortunately, the GIF may suffer from halo artifacts because the local linear model used in the GIF cannot represent the image well near some edges. In this paper, a gradient domain guided image filter is proposed by incorporating an explicit first-order edge-aware constraint. The edge-aware constraint makes edges be preserved better. To illustrate efficiency of the proposed filter, the proposed gradient domain guided image filter is applied for single image detail enhancement, tone mapping of high dynamic range (HDR) images and image saliency detection. Both theoretical analysis and experimental results prove that the proposed gradient domain guided image filter can produce better resultant images, especially near the edges where halos appear in the original GIF.**

***Index Terms*—Guided image filter, gradient domain, edge-preserving, detail enhancement, high dynamic range, saliency detection**

I. Introduction

Edge preserving smoothing is required by lots of applications in image processing, computation photography and computer vision, such as image detail enhancement [1], tone mapping of high dynamic range (HDR) images [2], joint upsampling [3], structure extraction from texture [4] and correspondence search [5]. With an edge-preserving smoothing algorithm, the details in the input image will be smoothed while the edges be preserved. The detail layer of the input image can also be obtained by subtracting the smoothed image from the input image. By amplifying the detail layer, a detail enhanced image is produced. Therefore, edge-preserving smoothing algorithms can also be used as edge-preserving enhancing/decomposition algorithms.

All the edge-preserving decomposition algorithms can be separated into two categories: one is local filter based algorithms such as median filter [6], bilateral filter (BLF) [7], its accelerated versions [2], [8], [9] and its iterative version [11], guided image filter (GIF) [10] and weighted guided image filter(WGIF) [17], the other is global optimization based algorithms such as total varition (TV) [12], its iterative shrinkage approach [13] and its extension [4], weighted least squares (WLS) [14] and its accelerated version, fast weighted least squares (FWLS) [15], and L_0 norm gradient minimization [16]. The global optimization based filters always give better results. All these algorithms are obtained by solving an optimization problem. The optimization problem is formulated as combination of a fidelity term and a regularization smooth term. With different fidelity terms or different regularization terms, different methods are proposed and different results are established. All these problems are solved after a number of iterations, so these global optimization based algorithms are usually very time consuming. An interesting concept of texture removal filter was firstly proposed in [4], the structure texture of the image was removed via solving a total variation based optimization problem. In [21], a patch based solution was proposed. In [22], a bilateral texture filter was proposed to remove texture in images. In the rolling guidance filter [11], the joint bilateral filter was iteratively invoked a few times. As a result, the texture in the image are removed. The local filter based filters usually have better efficiency, but the resultant image may suffer from artifacts. Median filter, widely known as an image de-noise filter, can also be used as a simple edge-preserving decomposition filter. Weighted median filter [18] can filter images with the weight from a guidance image, but the the speed could be an issue. In [19], an interesting constant time weighted median filter was proposed. In [20], a novel fast weighted median filter was proposed, the fast implementation makes the weighted median filter more practical. Bilateral filtering (BLF) [7] processes images by combining a range filter with a domain filter to preserve edges. It is a simple and widely used weighted average filter, but it may suffer from gradient reversal artifacts near some edges when used for detail enhancement [2], [14]. Guided image filter (GIF) [10] was proposed to avoid gradient reversal artifacts and it is derived from a local linear model. The main idea is using a linear transform to represent the pixel values in a window. Different from other algorithms, the GIF computes the resulting image by taking the structure of a guidance image into consideration and it is one of the fastest edge-preserving smoothing filters. Nevertheless, the model can not represent the image well near some edges. As a result, there may be some halos in the images [10]. This happens in some GIF based applications and it is most apparent in the detail enhanced images obtained by the GIF. The halos reduce the visual quality of the resulting images, and thus it is the main drawback of the GIF. In [17], a weighted guided image filter (WGIF) was proposed to reduce the halo artifacts of the GIF. An edge aware factor was introduced to the constraint term of the GIF, the factor makes the edges preserved better in the result images and thus reduces the halo artifacts. However, zeroth-order (intensity domain) constraints are specified to get desired pixel values and first-order (gradient domain) constraints to smooth the pixel values in both the GIF and the WGIF. Since there are no explicit

This work has been supported by National Nature Science Foundation of China under the research project 51475017 and the China Scholarship Council.

Fei Kou and Weihai Chen are with the School of Automation Science and Electrical Engineering, Beihang University, Beijing, China 100191. Fei Kou is also with the School of Electrical and Electronic Engineering, Nanyang Technological University, Singapore 639798 (e-mail: koufei@buaa.edu.cn, whchen@buaa.edu.cn).

Changyun Wen is with the School of Electrical and Electronic Engineering, Nanyang Technological University, Singapore 639798 (e-mail: ecywen@ntu.edu.sg).

Zhengguo Li is with Signal Processing Department, Institute for Infocomm Research, Singapore 138632 (email: ezgli@i2r.a-star.edu.sg).

(Corresponding author: W. Chen.)

This article has been accepted for publication in a future issue of this journal, but has not been fully edited. Content may change prior to final publication. Citation information: DOI 10.1109/TIP.2015.2468183, IEEE Transactions on Image Processing

constraints to treat edges in both of them, they cannot preserve edges well in some cases because they consider image filtering process and edge-preserving process together. It is widely believed that gradients are integral to the way in which human beings perceive images, and human cortical cells could be hard wired to preferentially respond to high contrast stimulus in their receptive fields [23], which directly correlate with gradients in an image. It is thus desired to design a new local filter which has explicit constraints to treat edges so as to make the gradient of the input image and output image be more similar.

In this paper, a gradient domain guided image filter is proposed by incorporating an explicit first-order edge-aware constraint. The proposed filter is based on local optimization and the cost function is composed of a zeroth order data fidelity term and a first order regularization term. The regularization term includes an explicit edge aware constraint which is different from the regularization terms in both the GIF [10] and the WGIF [17]. As a result, the factors in the new local linear model can represent the images more accurately near edges. Edges are preserved much better. In addition, compared with the WGIF in [17], the edge-aware factor is multi-scale while it is single scale in the WGIF. The large scale weight cooperates with the small scale weight proposed in the WGIF, becoming a multi-scale weight. The multi-scale factor can separate edges of an image from fine details of the image better. So the performance is highly improved, especially when fine details of an image is enhanced. Similar to the GIF in [10] and the WGIF in [17], the proposed filter also avoids gradient reversal. In addition, the complexity of the proposed filter is $O(N)$ for an image with N pixels which is the same as that of the GIF in [10] and the WGIF in [17]. These features allow many applications of the proposed filter in the fields of computational photography and image processing. The proposed filter is first applied for single image detail enhancement and tone mapping of HDR images. Experimental results of both applications show that the resultant algorithms produce images with better visual quality than both the GIF in [9] and the WGIF in [14]. Besides single image detail enhancement and tone mapping of HDR images, one new application is proposed in this paper, namely it is used as a post-processing tool for image saliency detection. Experimental results show the proposed gradient domain GIF can increase the accuracy of saliency detection.

The paper is organized as follows. Section II introduces the related works on guided image filtering. Then, the gradient domain guided image filtering is proposed in Section III. Followed by the applications and experimental results of the proposed filter in Section IV. Finally, Section V concludes this paper.

II. Related Works on Guided Image Filtering

In the GIF, there are a guidance image G and an image to be filtered X. They could be identical. Let $\Omega_{\zeta_1}(p)$ be a square window centered at a pixel p of a radius ζ_1. It is assumed that the output image $\hat{Z}$ is a linear transform of the guidance image G in the window $\Omega_{\zeta_1}(p')$ [24], [25]:

$$\hat{Z}(p) = a_{p'}G(p) + b_{p'}, \forall p \in \Omega_{\zeta_1}(p'), \tag{1}$$

where $a_{p'}$ and $b_{p'}$ are two constants in the window $\Omega_{\zeta_1}(p')$. Their values are obtained by minimizing a cost function $E(a_{p'}, b_{p'})$ which is defined as

$$E = \sum_{p\in\Omega_{\zeta_1}(p')} [(a_{p'}G(p) + b_{p'} - X(p))^2 + \lambda a_{p'}^2], \tag{2}$$

where λ is a regularization parameter penalizing large $a_{p'}$. The optimal values of $a_{p'}$ and $b_{p'}$ are computed as

$$a_{p'} = \frac{\mu_{G\odot X,\zeta_1}(p') - \mu_{G,\zeta_1}(p')\mu_{X,\zeta_1}(p')}{\sigma^2_{G,\zeta_1}(p') + \lambda}, \tag{3}$$

$$b_{p'} = \mu_{X,\zeta_1}(p') - a_{p'}\mu_{G,\zeta_1}(p'), \tag{4}$$

where $\odot$ is the element-wise product of two matrices. $\mu_{G\odot X,\zeta_1}(p')$, $\mu_{G,\zeta_1}(p')$ and $\mu_{X,\zeta_1}(p')$ are the mean values of $G \odot X$, G and X in the window $\Omega_{\zeta_1}(p')$, respectively.

The GIF is one of the fastest edge-preserving local filters and it outperforms the bilateral filter [7] in the sense that the GIF can avoid gradient reversal artifacts. However, the value of λ in the GIF [10] is fixed. As such, halos are unavoidable for the GIF in [10] when it is forced to smooth edges. A content adaptive GIF was proposed in [17] to overcome the problem. The cost function in Equation (2) is replaced by the following one:

$$E = \sum_{p\in\Omega_{\zeta_1}(p')} [(a_{p'}G(p) + b_{p'} - X(p))^2 + \frac{\lambda}{\Gamma_G(p')} a_{p'}^2], \tag{5}$$

where $\Gamma_G(p')$ is an edge aware weighting and it is defined by using local variances of 3×3 windows of all pixels as follows:

$$\Gamma_G(p') = \frac{1}{N}\sum_{p=1}^{N} \frac{\sigma^2_{G,1}(p') + \varepsilon}{\sigma^2_{G,1}(p) + \varepsilon}, \tag{6}$$

$\sigma^2_{G,1}(p')$ is the variance of G in the window $\Omega_1(p')$. ε is a small positive constant and its value is selected as $(0.001\times L)^2$ while L is the dynamic range of the input image. All pixels in the guidance image are used in the computation of $\Gamma_G(p')$. In addition, the weighting $\Gamma_G(p')$ measures the importance of pixel p' with respect to the whole guidance image. Due to the box filter in [10], the complexity of $\Gamma_G(p')$ is $O(N)$ for an image with N pixels.

The optimal values of $a_{p'}$ and $b_{p'}$ are computed as

$$a_{p'} = \frac{\mu_{G\odot X,\zeta_1}(p') - \mu_{G,\zeta_1}(p')\mu_{X,\zeta_1}(p')}{\sigma^2_{G,\zeta_1}(p') + \frac{\lambda}{\Gamma_G(p')}}, \tag{7}$$

$$b_{p'} = \mu_{X,\zeta_1}(p') - a_{p'}\mu_{G,\zeta_1}(p'). \tag{8}$$

The WGIF in [17] can be applied to reduce halo artifacts. However, both the GIF and the WGIF specify intensity-domain constraints (i.e., zeroth-order constraints) to obtain desired pixel values and gradient-domain constrains (i.e., first-order constraints) to smooth the pixel values over space and time. There are no explicit constraints to treat edges in both methods. Image filtering is usually an image coarsening

This article has been accepted for publication in a future issue of this journal, but has not been fully edited. Content may change prior to final publication. Citation information: DOI 10.1109/TIP.2015.2468183, IEEE Transactions on Image Processing

process accompanying with image smoothing. When image filtering and edge-preserving are considered together, edges may be smoothed inevitably. As a result, these edge-preserving methods cannot preserve edges well in some cases [26]. In the next section, a gradient domain GIF is introduced which includes an explicit first-order edge-aware constraint. The new constraint can be seamlessly integrated into the WGIF.

III. Gradient Domain Guided Image Filtering

Inspired by the Gradientshop in [26] and [27], a gradient domain GIF is introduced in this section. The proposed filter includes an explicit first-order edge-aware constraint and it thus preserves edges better than both the GIF and the WGIF.

A. A New Edge-Aware Weighting

A new edge-aware weighting $\hat{\Gamma}_G(p')$ is defined by using local variances of 3×3 windows and $(2\zeta_1+1)\times(2\zeta_1+1)$ windows of all pixels as follows:

$$\hat{\Gamma}_G(p') = \frac{1}{N}\sum_{p=1}^{N}\frac{\chi(p')+\varepsilon}{\chi(p)+\varepsilon}, \tag{9}$$

where $\chi(p')$ is defined as $\sigma_{G,1}(p')\sigma_{G,\zeta_1}(p')$, ζ_1 is the window size of the filter. It is usually set to 16 in detail manipulation applications. The weighting $\hat{\Gamma}_G(p')$ measures the importance of pixel p' with respect to the whole guidance image. Due to the box filter in [10], the complexity of $\hat{\Gamma}_G(p')$ is $O(N)$ for an image with N pixels.

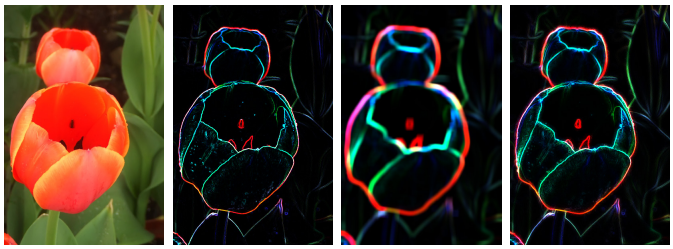

(a) Input image (b) $\Gamma_G(p')$ (c) $\Gamma_G(p')$ (d) $\hat{\Gamma}_G(p')$

Fig. 1: *Comparison of $\Gamma_G(p')$ and $\hat{\Gamma}_G(p')$. The window size of (b) and (c) are 3×3 and 33×33, respectively. 33 is selected here because the default ζ_1 in GIF is 16.*

The comparison of $\Gamma_G(p')$ and $\hat{\Gamma}_G(p')$ of an image are shown in Fig. 1. It is seen that, with this new weighting, the edges are detected more accurately. With the new weighting, one pixel will be detected as an edge pixel when both of its two scale variances are large. Compared with the weighting of the WGIF in [17], fewer details are detected as edges in the proposed multi-scale weighting. For example, there are more dots on the petals in Fig. 1(b) than Fig. 1(d), and the edges are much wider in Fig. 1(c) than Fig. 1(d). As a result, fine details are enhanced better by the proposed weighting. In addition, $\sigma_{G,\zeta_1}(p')$ is already calculated in the original GIF algorithm. So the new edge aware factor is more accurate than the factor in the WGIF with negligible increment of the computation time.

B. The Proposed Filter

It is shown in the linear model (1) that $\nabla\hat{Z}(p) = a_{p'}\nabla G(p)$. Clearly, the smoothness of $\hat{Z}$ in $\Omega_{\zeta_1}(p')$ depends on the value of $a_{p'}$. If the value of $a_{p'}$ is 1, the edge is then well preserved. This is expected if the pixel p' is at an edge. On the other hand, if the pixel p' is in a flat region, it is then expected that the value of $a_{p'}$ is 0 such that the flat region is well smoothed. Based on the observation, a new cost function is defined as

$$E = \sum_{p\in\Omega_{\zeta_1}(p')}[(a_{p'}G(p)+b_{p'}-X(p))^2+\frac{\lambda}{\hat{\Gamma}_G(p')}(a_{p'}-\gamma_{p'})^2], \tag{10}$$

where $\gamma_{p'}$ is defined as

$$\gamma_{p'} = 1-\frac{1}{1+e^{\eta(\chi(p')-\mu_{\chi,\infty})}}, \tag{11}$$

$\mu_{\chi,\infty}$ is the mean value of all $\chi(p)$. η is calculated as $4/(\mu_{\chi,\infty}-\min(\chi(p)))$. It is worth noting that the value of $\gamma_{p'}$ approaches 1 if the pixel p' is at an edge and 0 if it is in a smooth region. In other words, the value of $a_{p'}$ is expected to approach 1 if the pixel p' is at an edge and 0 if it is in a smooth region. As such, the proposed filter is less sensitive to the selection of λ. Subsequently, edges could be preserved better by the proposed filter than both the GIF and the WGIF.

The optimal values of $a_{p'}$ and $b_{p'}$ are computed as

$$a_{p'} = \frac{\mu_{G\odot X,\zeta_1}(p')-\mu_{G,\zeta_1}(p')\mu_{X,\zeta_1}(p')+\frac{\lambda}{\hat{\Gamma}_G(p')}\gamma_{p'}}{\sigma^2_{G,\zeta_1}(p')+\frac{\lambda}{\hat{\Gamma}_G(p')}}, \tag{12}$$

$$b_{p'} = \mu_{X,\zeta_1}(p')-a_{p'}\mu_{G,\zeta_1}(p'). \tag{13}$$

The final value of $\hat{Z}(p)$ is given as follows:

$$\hat{Z}(p) = \bar{a}_pG(p)+\bar{b}_p, \tag{14}$$

where $\bar{a}_p$ and $\bar{b}_p$ are the mean values of $a_{p'}$ and $b_{p'}$ in the window, respectively computed as

$$\bar{a}_p = \frac{1}{|\Omega_{\zeta_1}(p)|}\sum_{p'\in\Omega_{\zeta_1}(p)}a_{p'}\ ;\ \bar{b}_p = \frac{1}{|\Omega_{\zeta_1}(p)|}\sum_{p'\in\Omega_{\zeta_1}(p)}b_{p'}, \tag{15}$$

and $|\Omega_{\zeta_1}(p')|$ is the cardinality of $\Omega_{\zeta_1}(p')$.

C. Analysis of the Proposed Filter

For easy analysis, the images X and G are assumed to be the same. Two cases are studied as below.

1) The pixel p' is at an edge. The value of $\gamma_{p'}$ is usually 1. The value of $a_{p'}$ is computed as

$$a_{p'} = \frac{\sigma^2_{G,\zeta_1}(p')+\frac{\lambda}{\hat{\Gamma}_G(p')}}{\sigma^2_{G,\zeta_1}(p')+\frac{\lambda}{\hat{\Gamma}_G(p')}} = 1. \tag{16}$$

The value of $a_{p'}$ is 1 regardless of the value of λ. Clearly, the value of $a_{p'}$ is closer to 1 than both $a_{p'}$ in the GIF [10] and $a_{p'}$ in the WGIF [17] if the pixel p' is at an edge. This implies that sharp edges are preserved better by the proposed filter than both the GIF and the WGIF.

This article has been accepted for publication in a future issue of this journal, but has not been fully edited. Content may change prior to final publication. Citation information: DOI 10.1109/TIP.2015.2468183, IEEE Transactions on Image Processing

2) The pixel p' is in a flat area. The value of $\gamma_{p'}$ is usually 0 and the value of $\hat{\Gamma}_G(p')$ is usually smaller than 1. The value of $a_{p'}$ is computed as

$$a_{p'} = \frac{\sigma^2_{G,\zeta_1}(p')}{\sigma^2_{G,\zeta_1}(p') + \frac{\lambda}{\hat{\Gamma}_G(p')}}. \quad (17)$$

Since the value of $a_{p'}$ is 1 regardless of the choice of λ if the pixel p' is at an edge, a larger λ is selected in the proposed filter than the λ in the GIF and the WGIF because the selection will not affect the preservation of edges by the proposed filter. Obviously, this results in that the value of $a_{p'}$ is closer to 0 if the pixel p' is in a flat area. This means that the proposed filter smooth the flag area better than both the GIF and the WGIF.

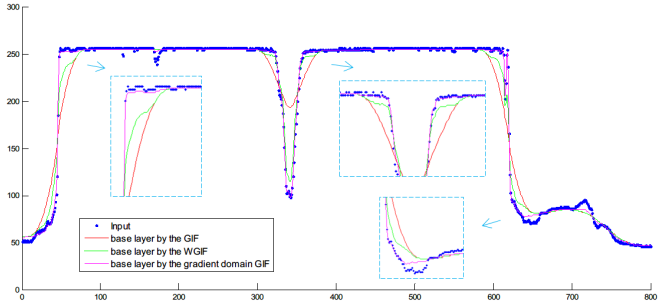

(a)

Fig. 2: *1-D illustration of the GIF, the WGIF and the proposed gradient domain GIF. $\zeta_1 = 16, \lambda = 1$ in all the three algorithm. The input data is obtained from the middle row of the red channel in Fig. 1 (a).*

To verify the analysis above, one smoothing result is presented. To better observe the difference, we only show the 1 dimension value. As shown in Fig.2, edges are preserved better by the proposed filter than both the GIF in [10] and the WGIF in [17]. From the zoomed-in patches showed in the figure, it is seen that the output values of the proposed filter are almost the same as the input values near edges while the output values of the GIF and the WGIF are far away from the input values. This proves our previous analysis that the gradient constraint can make the result more similar to the input data near edges. So the proposed gradient domain guided image filtering can preserve edges better than the GIF and the WGIF.

IV. Applications of the New Filter

In this section, the proposed gradient domain guided image filter is adopted to study single image detail enhancement, tone mapping of HDR images and saliency detection. Readers are invited to read the electronic version with full-size figures in order to better appreciate the differences among images.

A. Single Image Detail Enhancement

Single image detail enhancement is a typical example to compare performance of different filters from both the halo artifacts and the gradient reserve artifacts point of view. The filter image and the guidance image are identical for single image detail enhancement. The output image of the proposed filter would be an edge-preserved smoothing image. Then the detail layer of the input image can be obtained by calculating the difference between the input image and the output image. A detail enhanced image will be produced by amplifying the detail layer. In the following, we add four times of the detail layer to the input image to get the detail enhanced image.

(a) $\lambda = 0.01^2$ (b) $\lambda = 0.05^2$ (c) $\lambda = 0.1^2$ (d) $\lambda = 0.2^2$

Fig. 3: *Comparison of the selection of parameter λ. The images of each row are the detail layers of GIF, the detail enhancement results of GIF, the detail layers of the proposed filter, and the detail enhancement results of the proposed filter.*

First we compare the selection of parameter λ in Eq. 10 and the λ in the GIF. The results are shown in Fig. 3. From left to right, it can be seen that with the increasing of λ, there will be more details in the detail layer and this results in a sharper detail enhanced image. On the other hand, it may cause more halo artifacts near the edges (e.g. around the flower, green, black artifacts) for larger λ.

At the same time, the difference between the proposed filter and the GIF can be seen in Fig. 3. There are more edges in

This article has been accepted for publication in a future issue of this journal, but has not been fully edited. Content may change prior to final publication. Citation information: DOI 10.1109/TIP.2015.2468183, IEEE Transactions on Image Processing

(a) GIF (b) WGIF (c) the Proposed (d) BLF (e) L_0 (f) FWLS

Fig. 4: *Comparison of detail enhancement results.The images of each row are the detail enhanced images, the detail layers and two sets of zoom-in patches of the detail enhanced image, respectively.* $\lambda = 0.1^2$ *in the GIF and in the WGIF,* $\lambda = 0.15^2$ *in the proposed filter,* $\sigma_s = 16, \sigma_r = 0.1$ *for the BLF,* $\lambda = 0.01$ *in the L0 smoothing, and* $\sigma = 0.01, \lambda = 30^2$ *in the FWLS. The window size in the GIF, WGIF, BLF and the proposed filter are* 33×33.

TABLE I: *Scores of detail enhanced images by the GIF and the proposed filter*

	Input	0.01^2	0.05^2	0.1^2	0.2^2
GIF	36.87	38.97	40.25	34.33	28.86
Proposed	36.87	37.69	43.26	43.21	41.39

the detail layer decomposed by the GIF than by the proposed gradient domain GIF. The same as the GIF, the results of the proposed filter are sharper with the increasing of λ. However, it can be seen that the result of proposed algorithm has less artifacts even with a larger λ. In this case, we can use a larger λ with the proposed filter without worrying about the halo artifacts.

Next we use the blind object image quality metric in [28] to evaluate the detail enhanced image quality. The scores with this metric of the input and result images shown in Fig. 3 are given in the following table:

With this metric, a higher value represents a higher quality. Clearly, the proposed gradient domain outperforms the original GIF in [10]. From the table, we can also get that the score initially increases and then decreases as λ increases. This is because over-sharpened images may be resulted from excessively large values of λ, which are unnatural. At the same time, only the scores of two images generated by the original GIF are higher than the input image, whereas all the four images generated by the proposed gradient domain GIF have higher scores than the input image. Again, this shows we can use a larger λ with the proposed filter without worrying about the halo artifacts.

Now the proposed filter is compared with the GIF in [10], the WGIF in [17], the BLF in [7], the L_0 norm minimization in [16] and the FWLS in [15]. From the detail enhanced image shown in the first row of Fig. 4, it is seen almost all the algorithms (except L_0 minimization because it is a sparse based algorithm) produce similar results with overall view, the differences are edges. From the detail layers shown in the second row of Fig. 4, it is seen that the result of the WGIF is better than the original GIF, the BLF, the L_0 minimization and

This article has been accepted for publication in a future issue of this journal, but has not been fully edited. Content may change prior to final publication. Citation information: DOI 10.1109/TIP.2015.2468183, IEEE Transactions on Image Processing

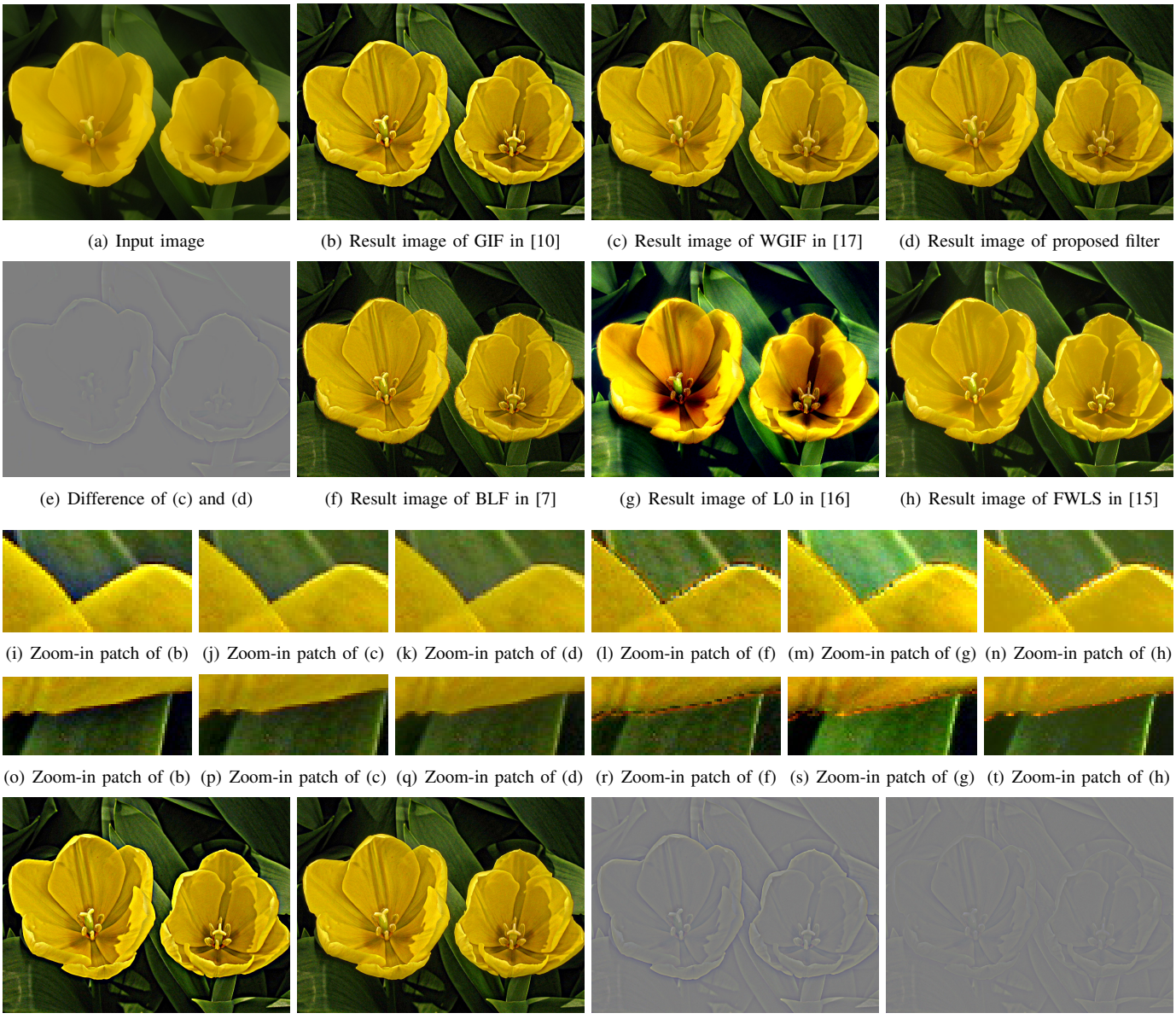

(a) Input image (b) Result image of GIF in [10] (c) Result image of WGIF in [17] (d) Result image of proposed filter

(e) Difference of (c) and (d) (f) Result image of BLF in [7] (g) Result image of L0 in [16] (h) Result image of FWLS in [15]

(i) Zoom-in patch of (b) (j) Zoom-in patch of (c) (k) Zoom-in patch of (d) (l) Zoom-in patch of (f) (m) Zoom-in patch of (g) (n) Zoom-in patch of (h)

(o) Zoom-in patch of (b) (p) Zoom-in patch of (c) (q) Zoom-in patch of (d) (r) Zoom-in patch of (f) (s) Zoom-in patch of (g) (t) Zoom-in patch of (h)

(u) Result image of the WGIF with large $\lambda = 0.5^2$ (v) Result image of the proposed filter with large $\lambda = 0.5^2$ (w) Detail layer of the WGIF with large $\lambda = 0.5^2$ (x) Detail layer of the proposed filter with large $\lambda = 0.5^2$

Fig. 5: *Comparison of detail enhancement results.*$\lambda = 0.1^2$ *in the GIF and in the WGIF,* $\lambda = 0.15^2$ *in the proposed filter,* $\sigma_s = 16, \sigma_r = 0.1$ *for the BLF,* $\lambda = 0.01$ *in the L0 smoothing, and* $\sigma = 0.01, \lambda = 30^2$ *in the FWLS. The window size in the GIF, WGIF, BLF and the proposed filter are* 33×33.

the FWLS. There are less edges in the detail layer of the WGIF than the others, but they are still much more apparent than the detail layer generated by the proposed filter. It is worth noting that the λ value in the proposed method is larger than the values of λ in both the GIF and the WGIF. We can conclude from Fig. 3 that a larger λ may produce more artifacts, but a larger λ in the proposed gradient domain GIF produce less artifacts than the GIF and the WGIF. From the zoom-in patches shown in Fig. 4, it is observed that the results of the proposed filter has less artifacts than all the other algorithms. There are halo artifacts in the results of the GIF, the WGIF and the BLF, while there are reversal artifacts in the results of the BLF, the l_0 minimization smoothing and the FWLS, but the proposed filter produces neither halo artifacts nor reversal artifacts.

From Figs. 5(a)-(t), the same conclusion can be drawn. The difference between Fig. 5 (c) and Fig. 5 (d) is presented in Fig. 5 (e). It can be seen that the differences are mainly near edges. There are more halos in Fig. 5 (c) than Fig. 5 (d).

To better compare the WGIF and the proposed gradient domain GIF, one more set of images are shown in Figs. 5(u)-(x). These images are generated with a large λ, by setting it to 0.5^2. It is seen that there are apparent black halos around the flowers in Fig. 5(u). From the detail layers shown in Figs. 5(w)-(x), it is observed that lots of edges are separated into the detail layer by the WGIF. This is the reason of the halo

This article has been accepted for publication in a future issue of this journal, but has not been fully edited. Content may change prior to final publication. Citation information: DOI 10.1109/TIP.2015.2468183, IEEE Transactions on Image Processing

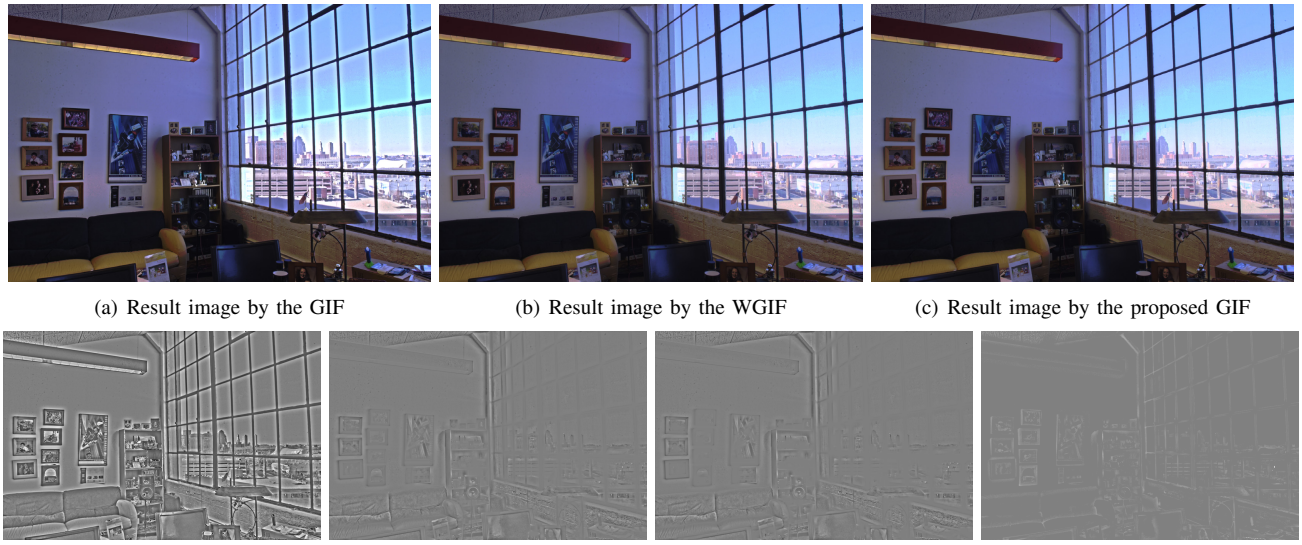

(a) Result image by the GIF (b) Result image by the WGIF (c) Result image by the proposed GIF

(d) Detail layer by the GIF (e) Detail layer by the WGIF (f) Detail layer by the proposed GIF (g) Difference of (e) and (f)

Fig. 6: *Comparison of tone mapping results of HDR image "office". The parameters are* $\zeta_1 = 15$, $\lambda = 1$ *for the GIF and the WGIF, and the parameters are* $\zeta_1 = 15$, $\lambda = 2$ *for the proposed filter.*

(a) Result image by the GIF (b) Result image by the WGIF (c) Result image by the proposed GIF

(d) Detail layer by the GIF (e) Detail layer by the WGIF (f) Detail layer by the proposed GIF (g) Difference of (e) and (f)

Fig. 7: *Comparison of tone mapping results of HDR image "belgium house". The parameters are* $\zeta_1 = 15$, $\lambda = 1$ *for the GIF and the WGIF, and the parameters are* $\zeta_1 = 15$, $\lambda = 2$ *for the proposed filter.*

artifacts. With our proposed gradient domain constraint, the edges are preserved in the base layer even if λ is very large, so there is no halo in the detail enhanced image. This implies that the proposed filter outperforms the WGIF in the sense that the proposed filter is less sensitive to the value of λ.

We also use the blind object image quality metric in [28] to compare different algorithms. The scores with this metric of the input and result images shown in Fig. 4 and 5 are summarized in the following table:

TABLE II: *Scores of enhanced images by different filters*

	Input	GIF	WGIF	Ours	BLF	L0	FWLS
Fig.4	36.9	34.3	40.7	42.4	39.6	36.1	33.7
Fig.5	29.7	27.8	37.1	44.9	35.5	32.2	28.2
Average	33.1	31.1	38.9	43.7	37.6	34.2	31.0

The results prove that the proposed gradient domain GIF is better than the original GIF in [10], the WGIF in [17], the BLF in [7], the L_0 norm minimization in [16] and the FWLS in [15].

This article has been accepted for publication in a future issue of this journal, but has not been fully edited. Content may change prior to final publication. Citation information: DOI 10.1109/TIP.2015.2468183, IEEE Transactions on Image Processing

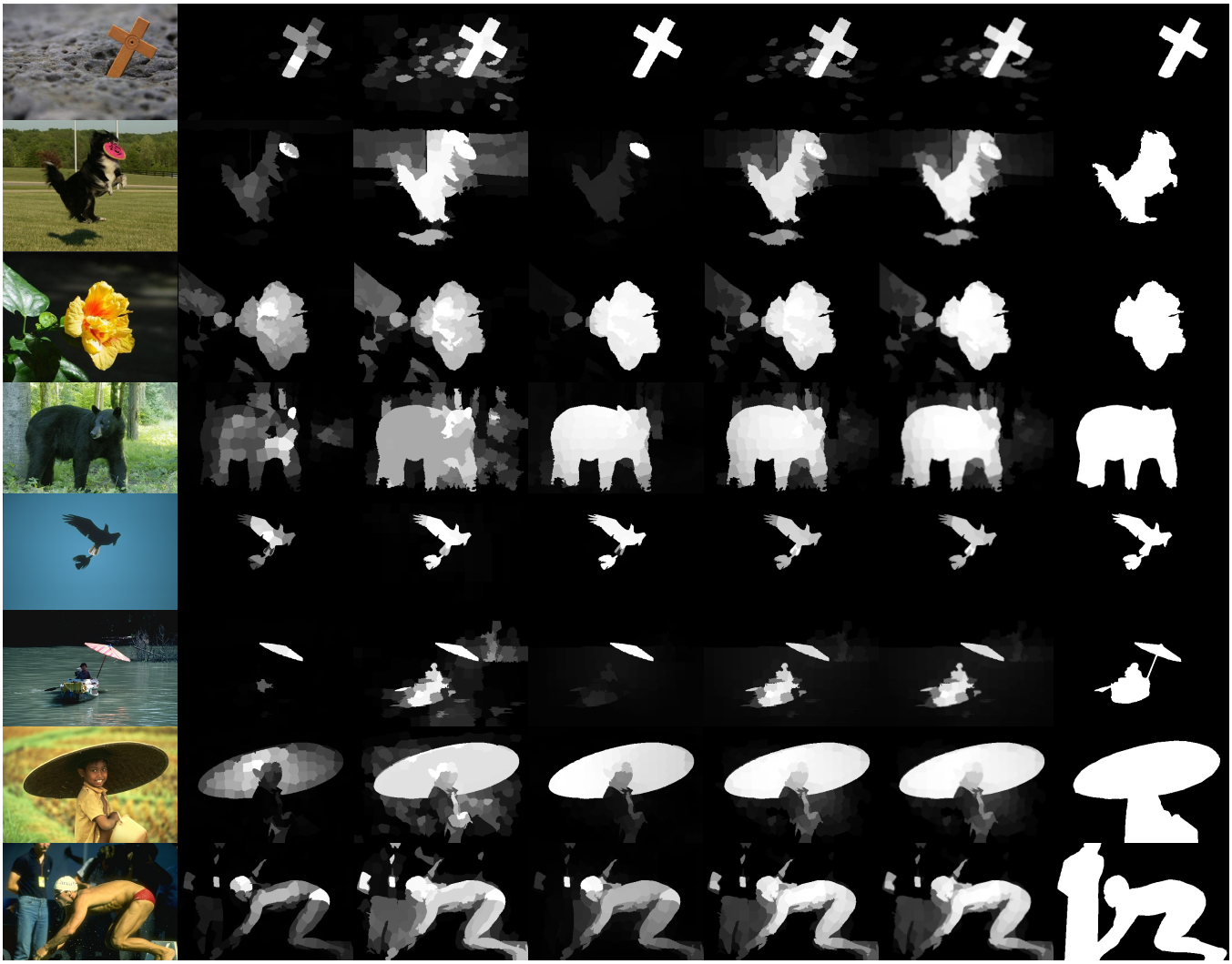

(a) Input image (b) SF (c) GS (d) MR (e) SO (f) Ours (g) Ground Truth

Fig. 8: *Comparison of saliency detection. The parameters are* $\zeta_1 = 1$, $\lambda = 0.1^2$ *for the proposed filter.*

B. Tone mapping of HDR images

Similar to single image detail enhancement, tone mapping of HDR images is a widely studied application to verify the performance of an edge-preserving image filter. So we also apply the proposed filter in HDR image tone mapping to compare with the other guided filter based algorithms.

HDR images are usually generated from several differently exposed images of the same scene, so an HDR image has more information than each of the differently exposed images. Limited by the dynamic range of monitors and printers nowadays, an HDR image has to be tone mapped to a low dynamic range (LDR) image. In an HDR tone mapping algorithm, the HDR image is first decomposed into a base layer and a detail layer, then the base layer is compressed and the detail layer is amplified. By adding up the compressed base layer and the amplified detail layer, a tone mapped LDR image is produced. The produced LDR image keeps most of the information in the HDR image with a much lower dynamic range. Similar to other tone mapping algorithms, the HDR image is decomposed to two layers by the proposed filter. The large contrast of the HDR image makes the variance change tremendously, so Gaussian blur is used to the variance before calculating the weight to make the result more natural.

Two sets of HDR tone mapping results are shown in Fig. 6 and Fig. 7. It is seen that the halo artifacts are very apparent in the results of the GIF in [10]. Even though the halo artifacts are reduced by the WGIF in [17], there are still visible halo artifacts. It is further improved by the proposed filter. The halo artifacts are more apparent to be observed from the detail image. For example, the edges in the windows in both Fig. 6 and Fig. 7 are more apparent in the results of the GIF and the WGIF than the proposed filter although the λ in the proposed filter is larger than the other two filters. Whereas there are more details in the result image of the proposed filter, for example, there are more textures on the floor in Fig. 7(c) than Fig. 7(b) produced by the WGIF. It is easier to be observed in the zoom-in patches in Fig. 7(b) and Fig. 7(c). It has been proven previously that a larger λ can produce more detailed image,

This article has been accepted for publication in a future issue of this journal, but has not been fully edited. Content may change prior to final publication. Citation information: DOI 10.1109/TIP.2015.2468183, IEEE Transactions on Image Processing

but may cause more halos in the guided filter based algorithm, so this demonstrates once again the proposed filter is better than the GIF and the WGIF. To observe the difference, the differences between the detail layer by the WGIF and by the proposed filter are also provided. For visualization purposes, the differences are amplified 5 times. It is seen that there are more halos in the results of the WGIF than the results of the proposed filter. We can conclude that the resultant image of the proposed filter generated with a larger λ has less halos but more details than the resultant image of the WGIF.

C. Image Salience Detection

The Gaussian filter is widely used in existing Saliency detection algorithms to refine Saliency maps. In this subsection, we will show that the proposed filter can be applied to improve the Saliency maps, even for the latest super-pixel based Saliency detection algorithm.

Visual saliency reflects how much a region stands out from the image. It has been a fundamental problem in image processing and computer vision with many applications, such as image compression [29], image cropping [30], tone mapping of HDR images [31], object detection and recognition [32].

In early stages, most saliency detection approaches are block based . Gaussian smoothing is widely used [33], [34] as a post-processing procedure to change the computed visual saliency image to a saliency map in salience detection algorithms. It can make the image smoother and reduce the effect of noises. Recently, many region-based approaches [35]–[38] are proposed with the development of superpixel algorithms [39], [40]. The Gaussian filter is no longer a suitable post-processing filter for saliency detection, because it may blur the edges of the saliency map. Superpixel algorithm is a roughly segmentation algorithm, so the objects may not be segmented correctly. In the following, a new post-processing method is introduced for the saliency detection algorithms which can improve the performance of these algorithms.

In [35], an optimization based saliency detection algorithm was proposed. The saliency optimization procedure can be adopted to many other superpixel based algorithm, such as [36]–[38]. Here the proposed filter is applied to further improve the algorithm in [35]. As a post-processing procedure, it can be adopted to almost all the saliency detection algorithms, especially the superpixel based algorithms.

After obtaining the final saliency map with the algorithm in [35], the saliency map is filtered with our proposed gradient domain guided image filter. The luminance channel of the input image is selected as the guidance image. With the proposed filter, the structure of the input image can be moved to the saliency map. This makes the pixels near edge separated more accurately. In addition, as the computational complexity is very low, negligible time is added. The running time is about 0.04 seconds for a 400*300 image on the computer with a Intel Core i7-3770 CPU @3.2GHZ and 8GB of RAM. Similar results can be obtained with other edge aware joint image filtering, including the GIF in [10], the WGIF in [17], the BLF in [7] and so on, but the GIF based algorithms usually have better computation efficiency.

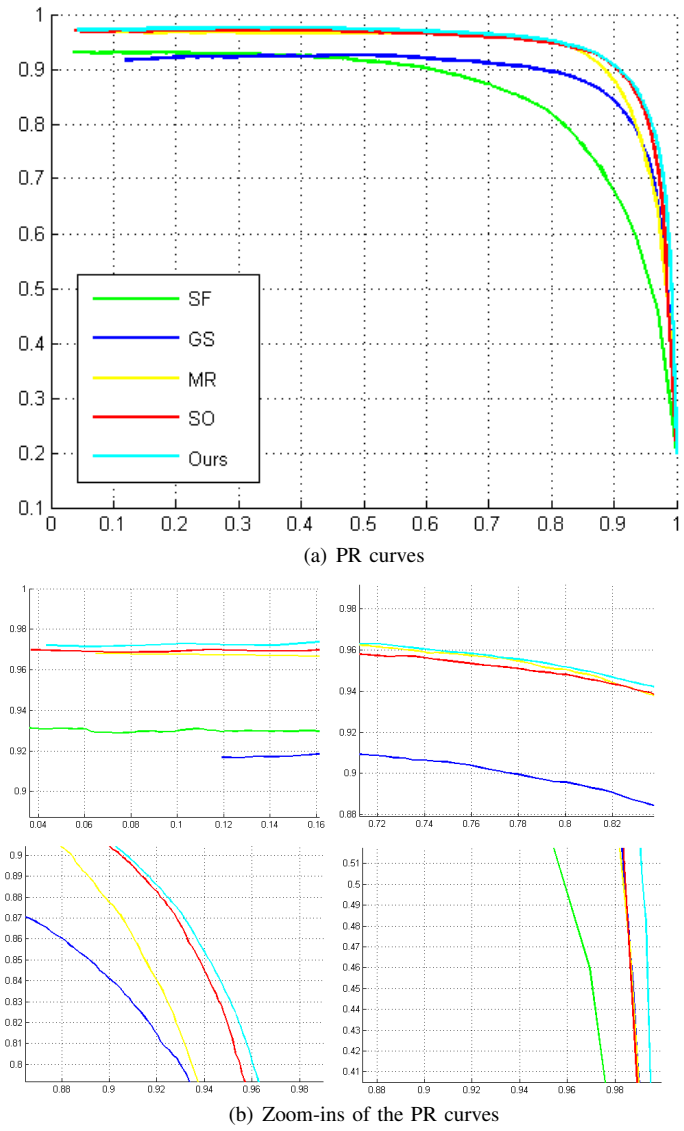

(a) PR curves

(b) Zoom-ins of the PR curves

Fig. 9: *PR curves comparison of saliency detection on dataset ASD*

Two datasets are tested to verify the proposed port-processing algorithm. The first dataset is the ASD dataset [41], in which 1000 images from the MSRA-B datasets [42] are labled with a binary pixel-wise object mask. The second dateset is the Berkeley Segmentation Dataset (BSD) dataset [43] with more complex scene. We compare the following four recently proposed saliency detection approaches: Saliency Filter (SF) [36], Geodesic Saliency (GS) [37], Manifold Ranking (MR) [38] and Saliency Optimization (SO) [35]. Four sets of images from each dataset are shown in Fig. 9. From all the images, it is seen that the edge shape of our algorithm is closer to the ground truth image, e.g., the lines of the cross are straighter.

Similar to many other saliency detection approaches, the precision-recall (PR) curves and the F-measure are adopted

This article has been accepted for publication in a future issue of this journal, but has not been fully edited. Content may change prior to final publication. Citation information: DOI 10.1109/TIP.2015.2468183, IEEE Transactions on Image Processing

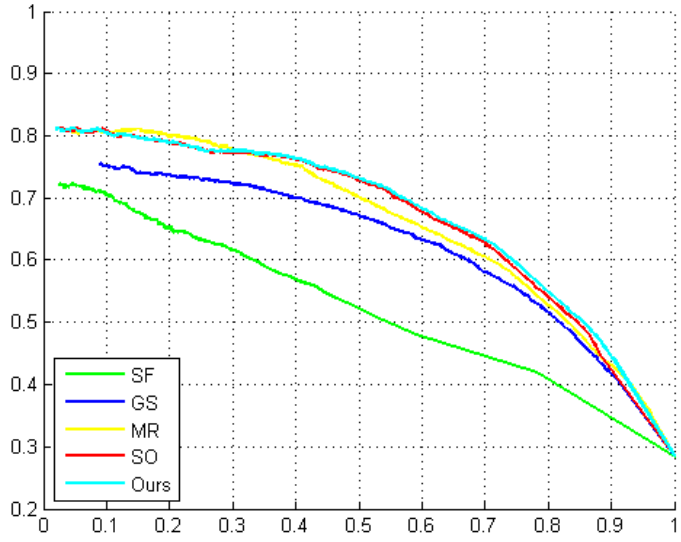

(a) PR curves

Fig. 10: *PR curves comparison of saliency detection on dataset BSD*

to quantitatively evaluate our contribution. Precision is the percentage of salient pixels correctly assigned, and recall is the percentage of the detected salient pixels compared with the ground truth image. The PR curves on ASD and BSD are shown in Fig. 9 and Fig. 10, respectively. It is seen that both the precision and recall are higher with our post-processing.

F-measure was proposed in [41]. In F-measure, an adaptive threshold is used. The threshold is calculated as

$$T_\alpha = \frac{2}{W \times H} \sum_{x=1}^{W} \sum_{y=1}^{W} S(x, y) \tag{18}$$

where x and y are the spatial pixel indexes of the saliency map S, W and H are the width and height of S, receptively. In saliency detection, the F_β is widely used. It is defined as

$$F_\beta = \frac{(1 + \beta^2) \cdot Precision \cdot Recall}{\beta^2 \cdot Precision + Recall} \tag{19}$$

Similar to other results [35]–[38], the value of β^2 is set as 0.3. The F-measures of the original and the proposed are 0.8784, 0.8789 on dataset ASD and they are 0.6448, 0.6480 on dataset BSD. This proves our post-processing algorithm can indeed improve the performance.

Finally, we compare several existing edge-preserving filters with the proposed filter as post-processing tool for saliency detection. The comparison algorithms are the bilateral filter (BLF) [7], the weighted median filter (WMF) in [20] and the rolling guidance filter (RGF) in [11]. The PR curves of these filters are shown in Fig. 11. From the PR curves of the different algorithms, we can draw a conclusion that all these filters can yield comparable results in improving the saliency detection. This is a new application of edge-preserving filters.

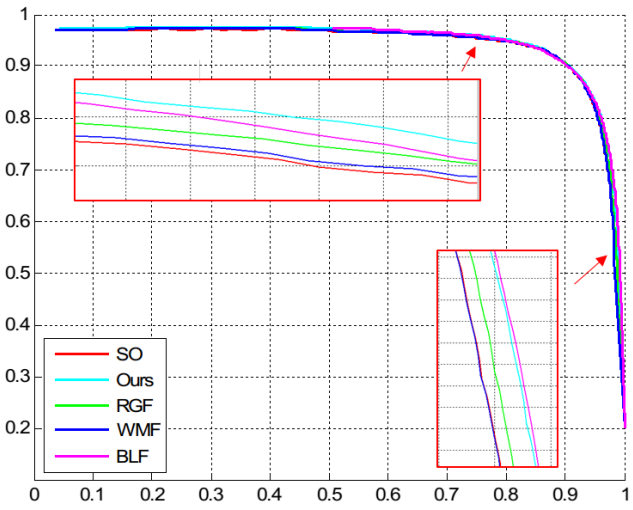

(a) PR curves on ASD

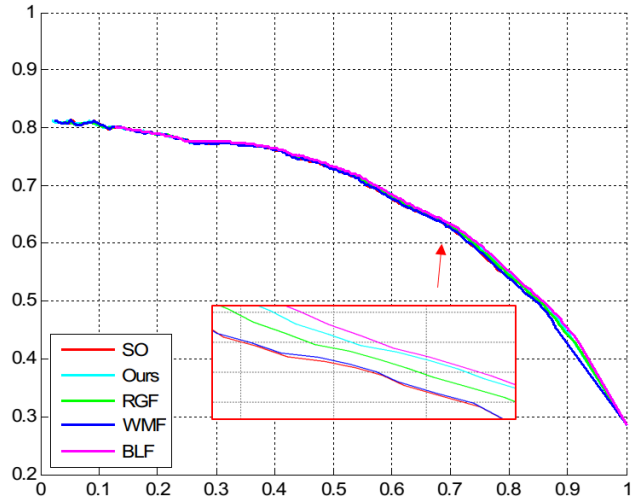

(b) PR curves on BSD

Fig. 11: *Comparison of different filters. The parameters are* $\zeta_1 = 1$, $\lambda = 0.1^2$ *for the proposed filter,* $\sigma_s = 3$, $\sigma_r = 0.05$, *iteration = 4 for the rolling guidance filter,* $r = 3$, $\sigma = 25.5$ *for the weighted median filter and* $\sigma_s = 3$, $\sigma_r = 0.05$ *for the bilateral filter.*

V. Conclusion And Remarks

In this paper, a new gradient domain guided image filter has been proposed by incorporating an explicit first-order edge-aware constraint into the existing guided image filter. Experimental results of image detail enhancement and HDR image tone mapping show that the proposed filter produces images with better visual appearance than the existing guided filter based algorithms, especially around edges. In addition, based on the new filter, a new saliency detection post-processing method has been proposed, which can make the saliency detection algorithms more accurate. It is reported in [10] that there are many applications of guided image filter such as the Flash/no-flash, RGB/NIR, dark-flash image restoration applications. We believe that the proposed filter

This article has been accepted for publication in a future issue of this journal, but has not been fully edited. Content may change prior to final publication. Citation information: DOI 10.1109/TIP.2015.2468183, IEEE Transactions on Image Processing

is also applicable to those applications. One more interesting problem is on the extension of the proposed filter so as to extract fine details from multiple images simultaneously by the extended filter as in [44], [45]. They will be studied in our future research.

REFERENCES

[1] Z. Farbman, R. Fattal, D. Lischinski, and R. Szeliski, "Edge-preserving decompositions for multi-scale tone and detail manipulation," In *ACM SIGGRAPH 2008*, pp. 1-10, Aug. 2008, USA.

[2] F. durand, and J. Dorsey, "Fast bilateral filtering for the display of high-dynamic-range images," Acm Trans. on Graphics, vol. 21, no. 3 pp. 257-266, Jul. 2002, USA.

[3] J. Kopf, M. F. Cohen, D. Lischinski, and M. Uyttendaele, "Joint bilateral upsampling," In *ACM SIGGRAPH 2007*, pp. 96, Jul. 2007. USA.

[4] L. Xu, Q. Yan, Y. Xia, and J. Jia, "Structure extraction from texture via relative total variation," ACM Trans. on Graphics, vol. 31, no. 6, pp. 139, Nov. 2012.

[5] K. J. Yoon and I. S. Kweon, "Adaptive support-weight approach for correspondence search," IEEE Trans. on Pattern Analysis and Machine Intelligence, vol. 28, no. 4, pp. 650-656, Feb. 2006.

[6] R. C. Gonzalez and R. E.Woods, Digital Image Processing, 2nd ed. Upper Saddle River, NJ, USA: Prentice-Hall, 2002.

[7] C. Tomasi and R. Manduchi, "Bilateral filtering for gray and color images," In *1998 6th IEEE Int. Conf. on Computer Vision (ICCV1998)*, pp. 836-846, Jan. 1998. India.

[8] S. Paris, and F. Durand, "A fast approximation of the bilateral filter using a signal processing approach," *9th European Conference Computer Vision (ECCV 2006)*, pp. 568-580, 2006, Austria.

[9] F. Porikli,, "Constant time O(1) bilateral filtering," in *IEEE Conference on Computer Vision and Pattern Recognition (CVPR2008)*. pp.1-8, June 2008, USA.

[10] K. He, J. Sun, and X. Tang, "Guided image filtering," IEEE Trans. On Pattern Analysis and Machine Learning, vol. 35, no. 6, pp. 1397-1409, Jun. 2013.

[11] Q. Zhang, X. Shen, L. Xu, and J. Jia, "Rolling Guidance Filter," in *13th European Conference Computer Vision (ECCV 2014)*, pp. 815-830, Sep. 2014, Switzerland.

[12] L. I. Rudin, S. Osher, and E. Fatemi, "Nonlinear total variation based noise removal algorithms," Physica D, vol. 60, no. 1-4, pp. 259-268, Nov. 1992.

[13] O. V. Michailovich, "An Iterative Shrinkage Approach to Total-Variation Image Restoration, IEEE Trans. on Image Processing, vol. 20, no. 5, pp. 1281-1299, May. 2011.

[14] Z. Farbman, R. Fattal, D. Lischinshi, and R. Szeliski, "Edge-preserving decompositions for multi-scale tone and details manipulation", ACM Trans. on Graphics, vol. 27, no. 3, pp.249-256, Aug. 2008.

[15] D. Min, S. Choi, J. Lu, B. Ham, K. Sohn, and M. N. Do "Fast Global Image Smoothing Based on Weighted Least Squares" IEEE Trans. Image Processing, vol. 23, no. 12, pp. 5638-5653, Dec. 2014.

[16] L. Xu, C. Lu, Y. Xu and J. Jia, "Image smoothing via L_0 gradient minimization", ACM Trans. on Graphics, vol. 30, no. 6, Dec. 2011.

[17] Z. G. Li, J. H. Zheng, Z. J. Zhu, W. Yao, and S. Q. Wu, "Weighted guided image filtering," IEEE Trans. on Image Processing. vol. 24, no.1, pp. 120-129, Jan. 2015.

[18] L. Yin, R. Yang, M. Gabbouj, and Y. Neuvo, "Weighted median filters: a tutorial,", *IEEE Trans. on Circuits and Systems II: Analog and Digital Signal Processing*, vol. 43, no. 3, pp. 157-192, 1996.

[19] Z. Ma, K. He, Y. Wei, J. Sun, and E. Wu, "Constant time weighted median filtering for stereo matching and beyond," in *2013 IEEE International Conference on Computer Vision (ICCV)*, pp. 49-56, Dec. 2013, Australia.

[20] Q. Zhang, L. Xu, and J. Jia, "100+ Times Faster Weighted Median Filter (WMF)," in *2014 IEEE Conference on Computer Vision and Pattern Recognition (CVPR)*, pp. 2830-2837, Jun 2014, USA.

[21] L.Karacan, E Erdem, and A. Erdem, "Structure-preserving image smoothing via region covariances". in *ACM Trans. on Graphics* Vol. 32, No. 6, pp. 176:1C176:11, 2013.

[22] H. Cho, H. Lee, H. Kang, and S. Lee, "Bilateral texture filtering," in *ACM Trans. on Graphics*, vol. 33, no. 4, pp. 1-8, 2014.

[23] J. H. Reynolds and R. Desimone. "Interacting roles of attention and visual salience in V4," Neuron, vol. 37, no. 5, pp.53-63, Mar. 2003.

[24] A. Torralba and W. T. Freeman, "Properties and applications of shape recipes," In *2003 IEEE Computer Vision and Pattern Recognition (CVPR)*, pp. 383-390, Jun. 2003, USA.

[25] A. Levin, D. Lischinski, Y. Weiss, " A closed-form solution to natural image matting," IEEE Trans. On Pattern Analysis and Machine Intelligence, vol. 30, no.2, pp. 228-242, Feb. 2008

[26] M. Hua, X. Bie, M. Zhang, and W. Wang, "Edge-Aware Gradient Domain Optimization Framework for Image Filtering by Local Propagation," in *2014 IEEE Conference on Computer Vision and Pattern Recognition (CVPR)*, 2014, pp. 2838-2845, Jun 2014, USA.

[27] P. Bhat, C. L. Zitnick, M. Cohen, and B. Curless, "Gradientshop: a gradientdomain optimization framework for image and video filtering," ACM Trans. Graphics, vol. 29, no. 2, pp.10:1-10:14, Apr. 2010.

[28] A. K. Moorthy and A. C. Bovik, "A Two-Step Framework for Constructing Blind Image Quality Indices," *IEEE Signal Processing Letter*, vol. 17, no.5, pp.513-516, May. 2010.

[29] L. Itti, "Automatic foveation for video compression using a neurobiological model of visual attention," , IEEE Transa. on Image Processing, vol. 13, no. 10, pp. 1304-1318, Oct. 2004.

[30] L. Marchesotti, C. Cifarelli, and G. Csurka, "A framework for visual saliency detection with applications to image thumbnailing," in *2009 IEEE 12th International Conference on Computer Vision(ICCV)*, pp. 2232-2239, Sept. 2009, Japan.

[31] Z. G. Li. and J. H. Zheng, "Visual-salience-based tone mapping for high dynamic range images," IEEE Trans. on Industrial Electronics, vol. 61, no.12, pp. 7076-7082, Dec. 2014.

[32] C. Kanan and G. Cottrell, "Robust classification of objects, faces, and flowers using natural image statistics," in*2010 IEEE Conference on Computer Vision and Pattern Recognition (CVPR)*, pp. 2472-2479, Jun. 2010, USA.

[33] L. Itti, C. Koch, and E. Niebur, "A model of saliency-based visual attention for rapid scene analysis," IEEE Trans. on pattern analysis and machine intelligence, vol. 20, no. 11, pp. 1254-1259, Nov. 1998.

[34] P. Bian, and L. Zhang, "Visual saliency: a biologically plausible contourlet-like frequency domain approach," Cognitive neurodynamics, vol. 4, no. 3, pp. 189-198, Mar. 2010.

[35] W. Zhu, S. Liang, Y. Wei, and J. Sun, "Saliency optimization from robust background detection," in *2014 IEEE Conference on Computer Vision and Pattern Recognition (CVPR)*, pp. 2814-2821, Jun. 2014, USA.

[36] F. Perazzi, P. Krahenbuhl, Y. Pritch, and A. Hornung, "Saliency filters: Contrast based filtering for salient region detection," in *2012 IEEE Conference on Computer Vision and Pattern Recognition (CVPR),* pp. 733-740, Jun. 2012, USA.

[37] Y. Wei, F. Wen, W. Zhu, and J. Sun, "Geodesic saliency using background priors," in *2012 European Conference on Computer Vision (ECCV 2012)* pp. 29-42, Oct. 2012, Italy.

[38] C. Yang, L. Zhang, H. Lu, X. Ruan, and M.-H. Yang, "Saliency detection via graph-based manifold ranking," in *2013 IEEE Conference on Computer Vision and Pattern Recognition (CVPR)*, pp. 3166-3173, Jun. 2013, USA.

This article has been accepted for publication in a future issue of this journal, but has not been fully edited. Content may change prior to final publication. Citation information: DOI 10.1109/TIP.2015.2468183, IEEE Transactions on Image Processing

[39] A. Levinshtein, A. Stere, K. N. Kutulakos, D. J. Fleet, S. J. Dickinson, and K. Siddiqi, "Turbopixels: Fast superpixels using geometric flows," IEEE Trans. On Pattern Analysis and Machine Intelligence, vol. 31, no. 12, pp. 22902297, May. 2009.

[40] R. Achanta, A. Shaji, K. Smith, A. Lucchi, P. Fua, and S. Susstrunk, "Slic superpixels compared to state-of-the-art superpixel methods," IEEE Trans. On Pattern Analysis and Machine Intelligence, vol. 34, no. 11, pp. 2274-2282, Nov. 2012.

[41] R. Achanta, S. Hemami, F. Estrada, and S. Susstrunk, "Frequency-tuned salient region detection," in *2009 IEEE Conference on Computer Vision and Pattern Recognition(CVPR),* pp. 1597-1604, Jun. 2009, USA.

[42] T. Liu, Z. Yuan, J. Sun, J. Wang, N. Zheng, X. Tang, et al., "Learning to detect a salient object," IEEE Trans. on Pattern Analysis and Machine Intelligence, vol. 33, no. 2, pp. 353-367, Feb. 2011.

[43] D. R. Martin, C. C. Fowlkes, and J. Malik, "Learning to detect natural image boundaries using local brightness, color, and texture cues," IEEE Trans. on Pattern Analysis and Machine Intelligence, vol. 26, no. 5, pp. 530-549, May. 2004.

[44] Z. G. Li, J. H. Zheng, and S. Rahardja, "Detail-enhanced exposure fusion," IEEE Trans. on Image Processing, vol. 21, no 11, pp. 4672-4676, Nov. 2012

[45] Z. G. Li, J. H. Zheng, Z. J. Zhu, and S. Q. Wu, "Selectively detail-enhanced fusion of differently exposed images with moving objects," IEEE Trans. on Image Processing, vol. 23, no. 10, pp. 4372-4382, Oct. 2014

Changyun Wen (F'10) received the B.Eng. degree from Xi'an Jiaotong University, Xi'an, China, in 1983 and the Ph.D. degree from the University of Newcastle, Newcastle, Australia in 1990. From August 1989 to August 1991, he was a Research Associate and then Postdoctoral Fellow at University of Adelaide, Adelaide, Australia. Since August 1991, he has been with School of Electrical and Electronic Engineering, Nanyang Technological University, Singapore, where he is currently a Full Professor. His main research activities are in the areas of control systems and applications, intelligent power management system, smart grids, cyber-physical systems, complex systems and networks, model based online learning and system identification, signal and image processing.

Dr. Wen is an Associate Editor of a number of journals including Automatica, IEEE Transactions on Industrial Electronics and IEEE Control Systems Magazine. He is the Executive Editor-in-Chief of Journal of Control and Decision. He served the IEEE Transactions on Automatic Control as an Associate Editor from January 2000 to December 2002. He has been actively involved in organizing international conferences playing the roles of General Chair, General Co-Chair, Technical Program Committee Chair, Program Committee Member, General Advisor, Publicity Chair and so on. He received the IES Prestigious Engineering Achievement Award 2005 from the Institution of Engineers, Singapore (IES) in 2005.

He is a Fellow of IEEE, was a member of IEEE Fellow Committee from January 2011 to December 2013 and a Distinguished Lecturer of IEEE Control Systems Society from February 2010 to February 2013.

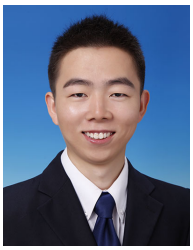

Fei Kou received his B.Eng. degree in Electronic Information Engineering from University of Science and Technology Beijing, Beijing, China, in 2010. He is currently working toward the Ph.D. degree at the School of Automation Science and Electrical Engineering, Beihang University, Beijing, China. Since July 2014, he has been working as a visiting Ph.D. student at the School of Electrical and Electronic Engineering, Nanyang Technological University, Singapore. His current research interests include image processing and computer vision.

Zhengguo Li (SM'03) received the B.Sci. and M.Eng. from Northeastern University, Shenyang, China, in 1992 and 1995, respectively, and the Ph.D. degree from Nanyang Technological University, Singapore, in 2001.

His current research interests include computational photography, mobile imaging, video processing & delivery, QoS, hybrid systems, and chaotic secure communication. He has co-authored one monograph, more than 160 journal/conference papers, and six granted patents, including normative technologies on scalable extension of H.264/AVC. He has been actively involved in the development of H.264/AVC and HEVC since 2002. He had three informative proposals adopted by the H.264/AVC and three normative proposals adopted by the HEVC. Currently, he is with the Agency for Science, Technology and Research, Singapore. He is an elected Technical Committee of the IEEE Visual Signal Processing and Communication. He served a General Chair of IEEE ICIEA in 2011, a Technical Brief Co-Chair of SIGGRAPH Asia in 2012, a General Co-Chair of CCDC in 2013, and the Workshop Chair of IEEE ICME in 2013. He was an Associate Editor of IEEE Signal Processing Letters since 2014.

Weihai Chen (M'00) received the B.Eng. degree from Zhejiang University, China, in 1982, and the M.Eng. and Ph.D. degrees from Beihang University, China, in 1988 and 1996, respectively. He has been with the School of Automation, Beihang University, as an Associate Professor from 1998 and as a Professor since 2007. He has published over 200 technical papers in referred journals and conference proceedings and filed 18 patents. His research interests include bio-inspired robotics, computer vision, image processing, precision mechanism, automation, and control.